Materials Research Proceedings 35 (2023) 302-309 https://doi.org/10.21741/9781644902714-36

Numerical evidence of submerged arc welding at changing of the main process parameters

Francesco Raffaele Battista[1,a *], Romina Conte[1,b], David Izquierdo Rodriguez[1,c], Francesco Gagliardi[1,d], Giuseppina Ambrogio[1,e] and Luigino Filice[1,f]

[1]Department of mechanical, energy and management engineering, University of Calabria, Rende (CS), Italy

[a]francesco.battista@unical.it, [b]romina.conte@unical.it, [c]david.rodriguez@unical.it, [d]francesco.gagliardi@unical.it, [e]giuseppina.ambrogio@unical.it, [f]luigino.filice@unical.it

Keywords: Assembly and Joining Processes, Arc Welding, FEM

Abstract. In the arc welding processes, the parts to be connected are subjected to thermal cycles that can generate distortions. Furthermore, owing to clamping constraints, residual stresses can arise affecting the mechanical properties of the welding bead. In the work proposed, multi-pass submerged arc welding (SAW) process was investigated by a numerical analysis, properly set by experimental evidence. Indeed, the welding bead of a reference sample, was section and etched before performing micrograph inspections to achieve the contours of both welded material and affected zone for each welding pass. Arc current, voltage and welding speed were the investigated process parameters. Their values were changed proportionally to maintain constant the generated specific heat of the process. Furthermore, the effect of different clamping set up was considered. As a result of the analysis, process configurations, according to the employed process parameters, able to reduce distortions and to minimize residual stress, were identified.

Introduction

Welding technologies are one of the most widespread joining processes in several industrial fields thanks to their flexibility, due to the many process alternatives currently available, and because they can be successfully applied to any material of engineering interest [1,2,3]. A fast localized heating of the material to melting temperature occurs during electric arc welding processes, followed by a rapid cooling phase. The main macroscopic effect of such thermal cycle results in an uneven distribution of displacements and thus in a deformed state of the welded joint [1,4,5]. The magnitude and distribution of welding-induced distortions negatively affect the aesthetic quality and dimensional accuracy of joints as well as may lead to additional post-weld processing [2,4,5,6]. Furthermore, the mechanical constraint action during process execution generates post-weld residual stresses. These can be critical because they adversely affect the fatigue strength of components and increase the risk of brittle fracture [2,4]. Both distortions and residual stresses in welded joints are influenced by numerous factors other than thermal cycle and clamping. Among these, the thermo-physical properties of the materials involved, the plate thickness, the welding method and parameters used, the sequence of passes, the joint configuration and the preheat and interpass temperatures deserve to be cited [3,4,5,7].

The mechanical restraint condition is one of the most significant factors affecting both the values and the distributions of welding deformations and residual stresses [1,5]. Indeed, numerous numerical-experimental studies attest that the sequence of constraints' application, as well as their location and dimension, results in changes in the displacement and tension fields [4,5]. In this regard, the degree of stiffness imposed on the components to be connected has a mirror effect on the post-weld strain and tension values [2]. In fact, in absence of clamping the welded parts have more possibility of movement and therefore high deformation and low internal post-welding stresses occur. Therefore, when planning a welding process, it is essential to identify the optimal

Materials Research Proceedings 35 (2023) 302-309 https://doi.org/10.21741/9781644902714-36

clamping condition that provides the right trade-off between deformations and internal stresses after cooling. Several FEM-based numerical simulation techniques are widely applied in order to optimize strain and tension fields in welded joints [1,2,4,5]. The strong interest in numerical simulation of welding-induced distortions and stresses has led to the development of several approaches for FEM modeling, from complex thermo-metallurgical-mechanical and thermo-mechanical models to simpler purely mechanical ones [1,6,8]. Welding processes numerical analysis enables fast, flexible, and cost-effective assessment of the effects of different process conditions and allows time and cost advantages related to the development and execution of additional experimental tests [2,9]. Indeed, through modern welding process numerical simulation techniques, it is possible to predict the final shape of the parts and then act at the planning stage of the process to match the required dimensional tolerances through compensation operations. Furthermore, numerical weld residual stresses assessment enables to carry out component service life estimates and/or predict areas where fatigue cracks can occur. Presently, among the most widely used FEM-based software for welding process simulation are ANSYS, ABAQUS and SYSWELD [1,4,5,9]. In particular, SYSWELD is a specially designed software for the simulation of welding processes and heat treatments and provides a wide range of tools and computational methods [1,3,7,9,10].

This paper deals with the numerical simulation of the submerged arc welding process on plates that differ in thickness and number of passes. The process numerical modeling and validation were carried out within SYSWELD software based on experimental tests. The main purpose of the work is to evaluate the effect produced on displacements and residual stress distributions by the different process configurations both in terms of plate thickness and process variables. Furthermore, the influence of experimental clamping on the investigated results was assessed compared with a process condition in the absence of clamping.

Material and Method

The experimental welding evidence was obtained joining ASTM A516 Gr. 70 steel plates. This is a C-Mn steel with excellent mechanical properties of notch toughness and is the standard specification for the fabrication of components subject to high pressure. As far as filler material is concerned, the low-carbon steel AWS 5.17 grade EH 14 was selected. This is a high Mn content, copper-coated wire commonly used in submerged arc welding. Two different sizes were used for the filler wire diameter, i.e., 2.4 mm for the root pass (pass 1) and 4 mm for all the others. The mechanical properties of the materials involved are reported in Table 1. As for the covering flux, ESAB OK Flux 10.61 was used.

Table 1 - Main mechanical properties of base material and filler metal.

	Tensile strength [MPa]	Yield strength (min) [MPa]	Elongation in 200 mm (min), %	Elongation in 50 mm (min), %
ASTM A516 Gr. 70	486 – 620	260	17	21
AWS 5.17 Gr. EH14	550	470	30	-

The experimental evidence involved multi-pass submerged arc welding of butt joints with different thicknesses. In particular, two different configurations were tested. The first experimental test concerned the joining of plates of 100 mm width, 400 mm length and, 10 and 20 mm thickness, respectively. While, the second trial involved plates of the same length and width as the previous ones but with thicknesses of 10 and 25 mm, respectively. In both tests, the plates were rigidly fixed at the edges along their whole length and thickness, over a width of 50 mm. The plates were neither subjected to initial pre-heating nor post-welding heat treatment, but an interpass temperature of 250°C was maintained between two consecutive passes.

Materials Research Proceedings 35 (2023) 302-309 https://doi.org/10.21741/9781644902714-36

Both experimental tests were performed using LINCOLN ELECTRIC's Place Power Wave® AC/DC 1000 SD CE welding machine and were carried out with reverse polarity DC. The first experimental test was carried out by a first root pass (pass 1) from the lower side of the plates, then two weld passes (pass 2 and 3) from the opposite side were enough to fill the whole milled channel previously made. Both passes 2 and 3 were performed employing the same values of voltage, current and welding speed. The second experimental test was carried out in the same manner and with the same process parameters as the first, to evaluate the effect of different plate thickness. Next, two more welding passes were performed to evaluate the effect of additional passes to strength the weld bead. Table 2 highlights the followed process sequences.

Table 2 - Main welding process parameters employed in the experimental tests.

Pass number	Voltage [V]	Current [A]	Welding speed [mm/min]
1	27	440	320
2	25.4	540	384
3	25.4	540	384
4	34	675	768
5	34	675	768

The experimental work also involved the obtainment of specimens from the welded samples to conduct macrographic inspections. The specimens were achieved through the steps of cutting, cold embedding, grinding, polishing and chemical etching. Then, the macrographs of the welds were achieved, through which the melted and heat-affected zones were identified for each pass. Fig. 1 shows the macrographs of the weld seams with the number of each pass highlighted.

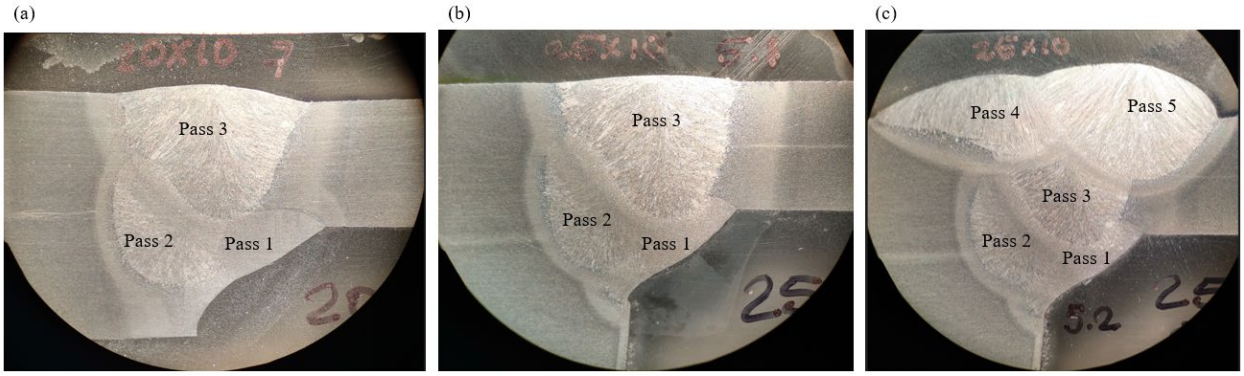

Fig. 1 - (a) Cross-sectional macrograph of the weld bead obtained from the first experimental test, (b) cross-sectional macrograph of the weld bead achieved from the second experimental test performed through three passes and (c) five passes.

Numerical modeling

A FEM model within SYSWELD software was developed based on the experimental evidence. Then an uncoupled sequential thermo-metallurgical mechanical analysis aimed at evaluating the welding-induced displacement and stress fields was conducted.

The first phase of numerical modeling involved the creation of 2D joint models. The FEM models of the tested specimens were developed in the Visual-mesh environment of the SYSWELD package. Due to computational time reasons, all FEM models were developed with a 100 mm length, while the other dimensions reflected those of the experimental specimens. Near the melted and heat affected zone, a finer mesh was made to obtain more accurate results. The FEM models of the three simulated process conditions are shown in Fig. 2.

Materials Research Proceedings 35 (2023) 302-309 https://doi.org/10.21741/9781644902714-36

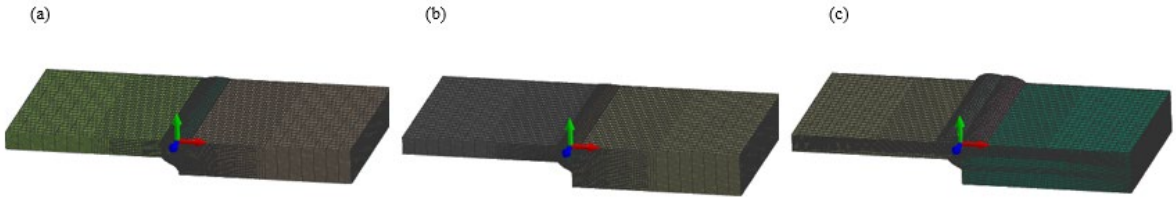

Fig. 2 – (a) 3D FEM model of the specimen related to the first experimental test, (b) 3D FEM model of the specimen related to the second experimental test performed with three passes and (c) five passes.

A transient thermal analysis was first carried out in the Visual-Weld environment through the moving heat source method already implemented within the software [11]. This kind of analysis is mainly affected by the availability of the physical materials properties at changing temperatures and the modeling of the heat source that simulates the arc movement [5,9,11]. Regarding temperature-dependent thermo-mechanical materials parameters such as thermal conductivity and yield stress were already implemented in the SYSWELD database. As an example, in Fig. 4 the trends of these properties at varying temperature and metallurgical phases for the base material extracted from the software have been shown [12]. The 3D double ellipsoid model proposed by Goldak [13] was employed for heat source modeling because it provides a reliable description of the heat distribution produced by the electric arc during welding [1,3]. Heat source design was performed for each welding pass based on the values of specific heat input, welding speed, process efficiency and the single pass sizes. The latter were obtained from the macrographic specimen analysis achieved by the experimental tests.

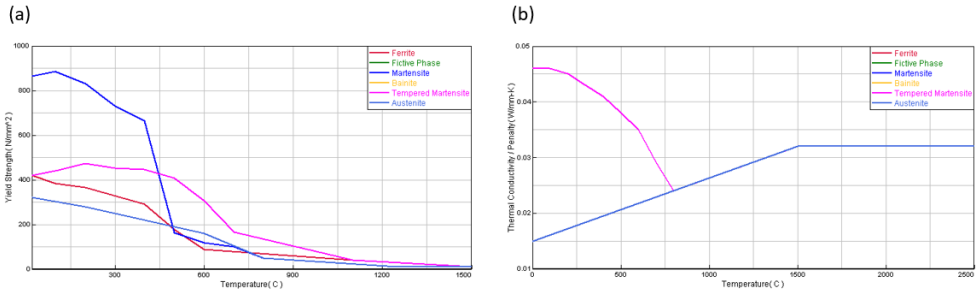

Fig. 3 - Trends of yield strength (a) and thermal conductivity (b) of ASME A516 Gr.70 steel as a function of temperature and metallurgical phases from the SYSWELD materials database [12].

To solve the thermal analysis, the cooling conditions were set in a way that the models' external surfaces exchanged heat by convection and radiation to the environment. For that, a room temperature of 20 °C was set. Since the subsequent mechanical analysis took as input the temperature field obtained as a result of the thermal analysis, the FEM models required validation by experimental data. Hence, heat source calibration was performed with the geometric parameters describing Goldak's model [13] that were iteratively changed for each pass until the predicted melted zone was in good agreement with that obtained from the macrographs. Fig. 4 shows the result of heat source calibration for each of the three simulated process conditions, while Table 3 shows the final numerical values of the parameters of Goldak's model that were subject to optimization. The geometric parameters are referred to the model proposed in the study [13], in addiction, it is specified that the root pass (pass1) was not simulated in the present investigation.

Materials Research Proceedings 35 (2023) 302-309 https://doi.org/10.21741/9781644902714-36

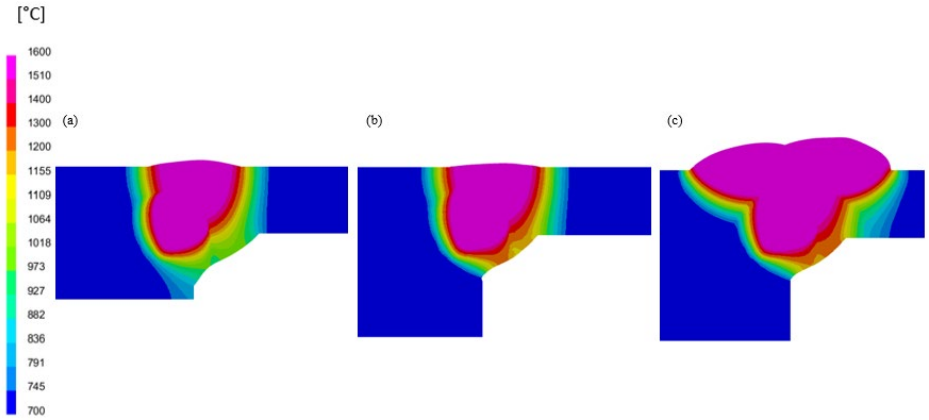

Fig. 4 - Melted and heat affected zone after calibration step for process conditions related to: (a) first experimental test, (b) second experimental test with three passes and (c) five passes.

Table 3 - Final values of the geometric parameters of Goldak's model according to the nomenclature of the study [13].

Pass Number	Test 1				Test 2			
	a [mm]	c1 [mm]	c2 [mm]	b [mm]	a [mm]	c1 [mm]	c2 [mm]	b [mm]
2	5.5	6.667	13.33	7	1.25	3.333	6.667	7
3	1.25	3.333	6.667	7.2	5.5	6.667	13.33	7
4					7	3.333	6.667	2
5					6	3.333	6.667	2

Based on the thermal analysis results carried out on the calibrated models, mechanical analysis was performed to predict post-cooling distortions and stresses. For this purpose, an elastic-plastic material behavior with isotropic hardening and small displacement theory was assumed. In this analysis the FEM models were rigidly constrained in the same manner as the experimental tests. Thereafter, a clamping-free condition was evaluated in view of analyzing its effects on the displacement and tension fields.

Results and discussion

The results of numerical simulations aimed to analyze the effect of different plate thickness and passes number on the displacements and residual stress distributions. Furthermore, the effect produced on the same output through the experimental clamping compared with a case without clamping was assessed.

The normal displacements and residual stresses after the cooling phase from the two experimental tests both performed with three passes were compared to evaluate the effect of different plate thicknesses. Figs 5 and 6 show the normal displacement and residual stresses at the end of welding for the same number of passes. As for the displacement field this appeared to be in good agreement between the two models, the only observable difference being lower values at the root pass in the case of the 10x25-thickness model (Fig. 5). The stress field between the two cases was also comparable. In the case of the thicker model, bead sections with slightly lower stress values were observed. Lower values for that model were also detected at the lower edge of the thicker plate (Fig. 6).

Materials Research Proceedings 35 (2023) 302-309 https://doi.org/10.21741/9781644902714-36

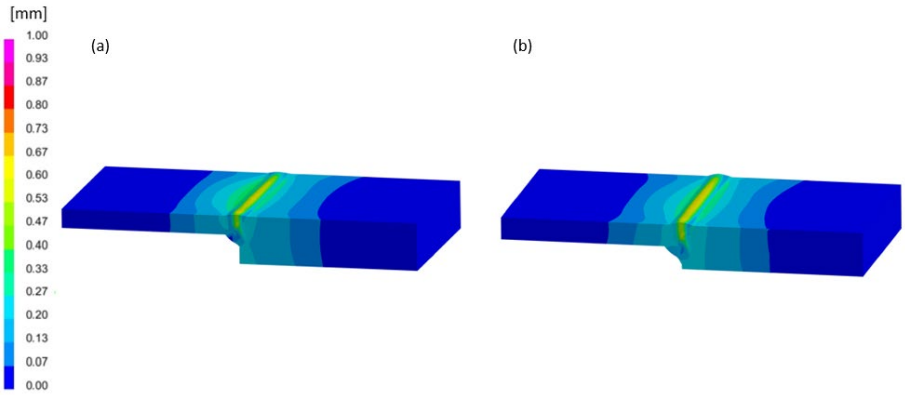

Fig. 5 - Post-weld displacement field for 10x20 mm (a) and 10x25 mm (b) thickness models.

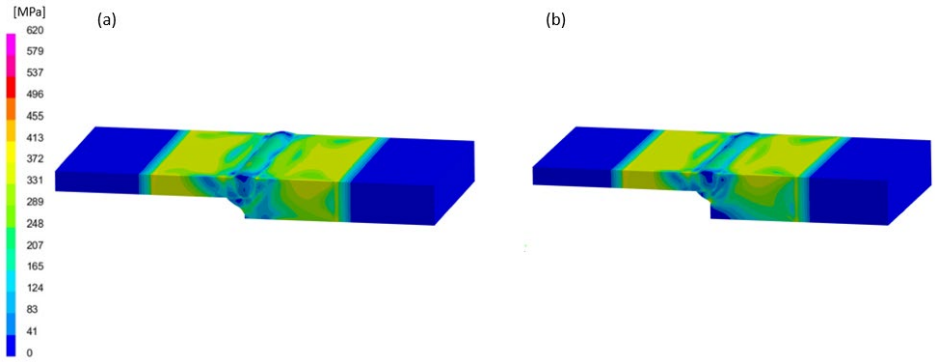

Fig. 6 - Post-weld stress field for 10x20 mm (a) and 10x25 mm (b) thickness models.

As for the influence of the different process parameters employed is concerned, the distortions and residual stresses of the second test performed with three and five passes, respectively, were compared. Fig. 7 shows the displacement fields for the second experimental test carried out with three and five passes, while Fig. 8 shows the post-welding residual stresses. The model performed with five passes compared with that using three produced an enlargement of the areas with higher value of the displacement field at the bead (Fig. 7). As for residual stresses, the weld bead produced by five passes exhibited slightly lower values at the areas adjacent to the bead not subject to the constraint. Low stress values were also observed at the surface portions of the bead, particularly for the last pass (Fig. 8).

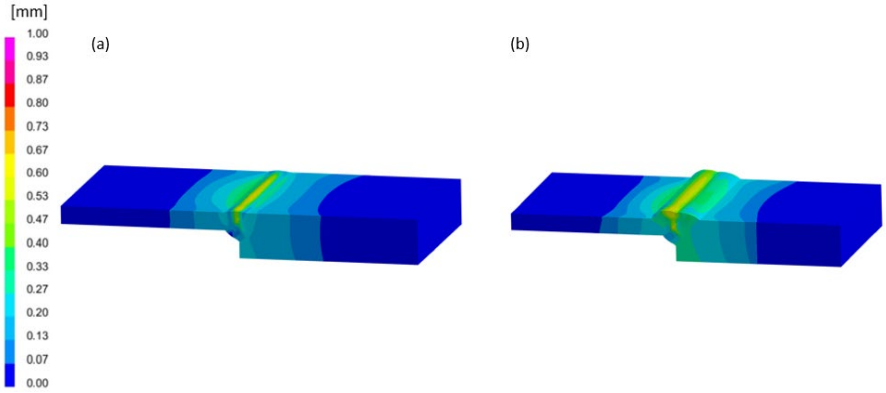

Fig. 7 - Post-weld normal displacements for the 10x25-thickness model performed with three (a) and five passes (b).

Materials Research Proceedings 35 (2023) 302-309 https://doi.org/10.21741/9781644902714-36

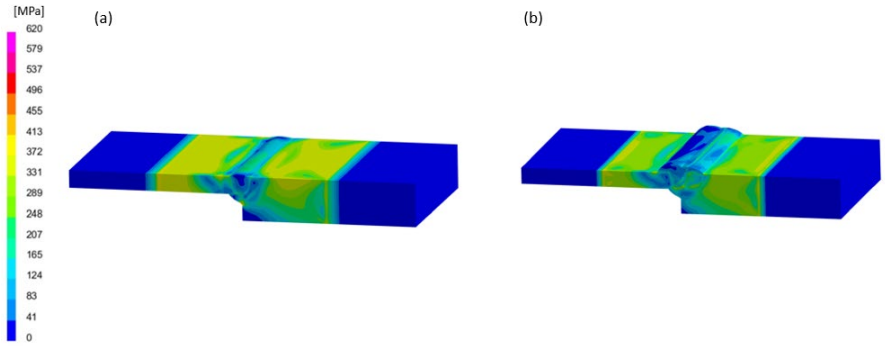

Fig. 8 - Post-weld residual stresses for the 10x25-thickness model performed with three (a) and five passes (b).

Finally, the FEM model related to the first experimental trial was considered in order to evaluate the effect of experimental clamping on the mechanical outputs investigated. In particular, the post-welding displacement and stresses were compared in the case of constrained sample as in the experimental tests and under free conditions. The latter condition was obtained by blocking model displacements on a lower edge of the thicker plate in the three directions of space. This prevents rigid motion of the body during numerical simulation and allows the possibility of free thermal expansion of the material. Fig. 9 show the post-welding normal displacement and residual stress fields for the examined model in the case of experimental clamping and without clamping. As can be observed from Fig. 9, much greater distortion is generated in the absence of clamping. The post-weld stress distribution also changes; a significant reduction in the extensions of the areas of greatest stress can be noticed.

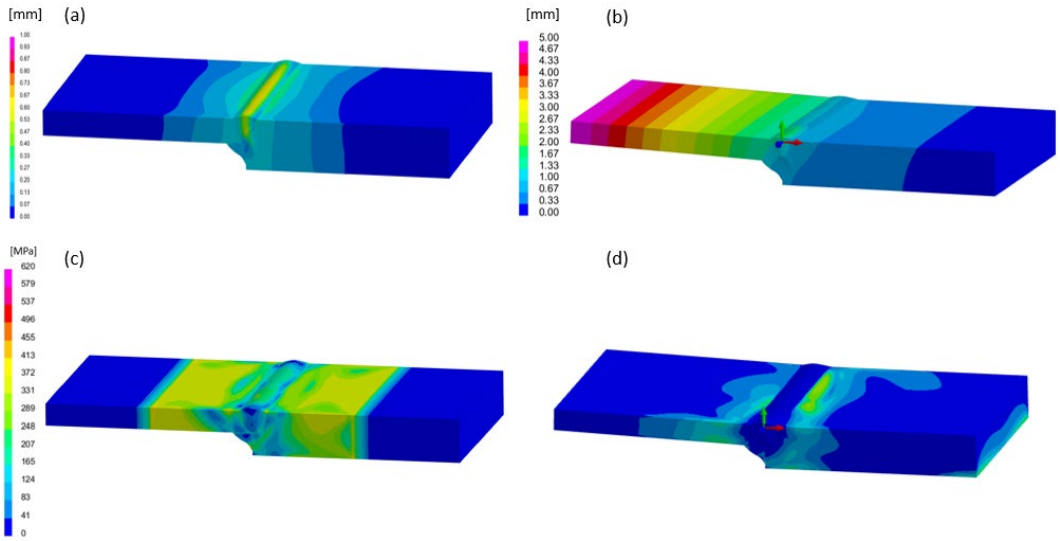

Fig. 9 – Post-weld normal displacements and residual stresses in the cases of experimental clamping (a) - (c) and without clamping (b) - (d).

Summary

This paper deals with the numerical simulation of the submerged arc welding process on plates with different thicknesses performed under different number of passes. The process numerical modeling and validation were carried out based on experimental tests. The study is aimed at evaluating the effect produced on the displacements and residual stress distributions by the different process configurations employed both in terms of plate thickness and process parameters. Moreover, the effect of the clamping condition applied in the experimental tests was assessed in

comparison with a case without clamping. Analysis of the results showed that the effect of the five-mm thickness difference between the plates involved is negligible in terms of both displacement range and post-welding residual stresses. Regarding the effect of process parameters, an enlargement around the bead area of the higher-value displacement field was observed in the case of welding by five passes. In addition, the effect of a higher number of passes is reflected by a slight reduction in the post-weld stress values in the areas adjacent to the bead free of constraints. Finally, it was observed that in the absence of clamping a much more pronounced deformation state is obtained, with maximum values approximately five times higher than in the experimental clamping case for the chosen investigated plates' dimensions. Furthermore, a significant reduction in high-stress areas adjacent to the bead was observed without clamping. The obtained evidence are in agreement with the experimental process knowing confirming the reliability of the employed numerical model.

References

[1] E. S.V. Marques, F. J.G. Silva, A. B. Pereira, Comparison of finite element methods in fusion welding processes - A review, Metals 10.1 (2020) 75. https://doi.org/10.3390/met10010075

[2] M. Slováček, T. Kik, Use of Welding Process Numerical Analyses as Technical Support in Industry. Part 1: Introduction to Welding Process Numerical Simulations. Biuletyn Instytutu Spawalnictwa. 4 (2015) 25-31. https://doi.org/10.17729/ebis.2015.4/3

[3] T. Kik, Computational techniques in numerical simulations of arc and laser welding processes. Materials 13.3 (2020) 608. https://doi.org/10.3390/ma13030608

[4] Y. Li et al, Effect of structural restraint caused by the stiffener on welding residual stress and deformation in thick-plate T-joints. J. of Mater. Res. and Tech. 21 (2022) 3397-3411. https://doi.org/10.1016/j.jmrt.2022.10.127

[5] D. Venkatkumar, D. Ravindran, Effect of boundary conditions on residual stresses and distortion in 316 stainless steel butt welded plate. High Temp. Mater. Proc. 38 (2019) 827-836. https://doi.org/10.1515/htmp-2019-0048

[6] D. Tikhomirov et al. Computing welding distortion: comparison of different industrially applicable methods. Advanced mater. research. Vol. 6. Trans Tech Pub. Ltd (2005) 195-202. https://doi.org/10.4028/www.scientific.net/AMR.6-8.195

[7] T. Kik, J. Górka, Numerical simulations of laser and hybrid S700MC T-joint welding. Materials 12.3 (2019) 516. https://doi.org/10.3390/ma12030516

[8] Z. Barsoum, M. Ghanadi, S. Balawi, Managing welding induced distortion-comparison of different computational approaches. Procedia Engineering 114 (2015) 70-77. https://doi.org/10.1016/j.proeng.2015.08.043

[9] A. A. Deshpande et al, Combined butt joint welding and post weld heat treatment simulation using SYSWELD and ABAQUS. Proceedings of the Institution of Mechanical Engineers, Part L: J. of Mater.: Design and Applications 225.1 (2011) 1-10. https://doi.org/10.1177/14644207JMDA349

[10] T. Kik, M. Slováček, M. Vaněk, Use of Welding Process Numerical Analyses as Technical Support in Industry. Part 2: Methodology and Validation. Biuletyn Instytutu Spawalnictwa 5 (2015) 25-32. https://doi.org/10.17729/ebis.2015.5/4

[11] L. Iorio (2021) ESI Welding simulation solution, ESI Group internal presentation.

[12] Welding Simulation User Guide, Sysweld Manual ESI Group.

[13] J. Goldak, A. Chakravarti, M. Bibby, A new finite element model for welding heat sources. Metallurgical transactions B 15 (1984) 299-305. https://doi.org/10.1007/BF02667333